19th Australasian Fluid Mechanics Conference
Melbourne, Australia
8-11 December 2014

Recent Progress in Explicit Shear-Eliminating Vortex Identification

V. Kolář[1] and J. Šístek[2]

[1]Institute of Hydrodynamics, Academy of Sciences of the Czech Republic
CZ-16612 Prague 6, Czech Republic

[2]Institute of Mathematics, Academy of Sciences of the Czech Republic
CZ-11567 Prague 1, Czech Republic

Abstract

All the widely used pointwise vortex-identification schemes based on the velocity-gradient tensor $\nabla\mathbf{u}$ (Q, λ_2, Δ, and λ_{ci}) *implicitly* suppress—unlike vorticity—the biasing effect of shear on their outcome. However, it is shown below that *explicit* shear-eliminating vortex-identification methods are in this regard more efficient in regions of strong shear. The latter ones are represented by the triple-decomposition method (TDM) and by the very recently proposed average-corotation scheme; their results, not mutually compared earlier, are remarkably similar.

Introduction

Although all the widely used pointwise vortex-identification schemes [1-7] sharing a basis in the velocity-gradient tensor $\nabla\mathbf{u}$ (Q, λ_2, Δ, and λ_{ci}) somehow suppress the biasing effect of shear, it is always achieved in an implicit manner. The first approach aiming at the explicit determination and elimination of a local shear—in terms of a portion of $\nabla\mathbf{u}$ labelled shear tensor—is the triple-decomposition method (TDM) [8]. TDM concentrates on tensor behaviour and employs the so-called basic reference frame (BRF), in which the effect of local shear near a point appears most significantly. However, the search for BRF represents an optimization problem for each point in the flow domain, which makes TDM computationally expensive. The new identification scheme introduced recently in [9], the average-corotation method, is based on the notion of local corotation of material line segments which is applicable to an arbitrary planar cross section going through the given point in a 3D flow. The local corotation of line segments near a point, as a planar concept, is directly related to the residual vorticity in 2D according to TDM. Both methods [8, 9] differ in 3D vortex identification: the residual vorticity tensor $\mathbf{\Omega}_{\mathrm{RES}}$ is employed according to TDM, while the corotation method employs the average-corotation vector $\boldsymbol{\omega}_{\mathrm{RAVG}}$. The vector $\boldsymbol{\omega}_{\mathrm{RAVG}}$ provides besides a well-defined kinematic interpretation in terms of corotation much faster numerical evaluation than TDM. Four different flow situations (a hairpin vortex of boundary-layer transition, the reconnection process of two Burgers vortices, a flow around an inclined flat plate, and a flow around a revolving insect wing) are analyzed in terms of the two explicit shear-eliminating schemes and two standard criteria, Q and λ_2. The paper concentrates on the following new aspects: (i) how strongly the 3D results of both explicit shear-eliminating methods resemble each other, (ii) how the two explicit shear-eliminating methods outperform Q and λ_2 in regions of strong shear near the plate or insect wing edges. All four methods presented below are briefly summarized in Appendix.

Vortex-Identification Results

For comparison purposes, the standard λ_2-criterion provides reference results for the following matching procedure described in [9]. After choosing a sufficiently low threshold level for the λ_2-method, we determine the corresponding threshold values for the other three methods under consideration (Q, and the two explicit shear-eliminating methods) by minimizing the characteristic ratio V_N/V_O over all possible thresholds. Here V_N corresponds to the volume where methods do not overlap in terms of vortex regions (i.e. one method detects a vortex while the other does not) and V_O denotes the overlapping volume (i.e. the volume representing a vortex according to both methods).

Hairpin Vortex of Boundary-Layer Transition

Boundary-layer transition to turbulence is one of very basic flow problems associated with distinct vortical structures like hairpin vortices. The examined DNS dataset deals with numerical simulation of wind-tunnel experiments using controlled disturbance excitation with frequency = 62.5 Hz at Re (based on the displacement thickness) of 730, according to [10]. Figure 1 shows a single hairpin vortex formed during the transition process to turbulent boundary layer. The adopted matching procedure [9] shows high similarity of results for all four considered vortex-identification methods.

Reconnection Process of Two Burgers Vortices

The subsonic DNS dataset for the reconnection process of two Burgers vortices at Ma = 0.3 and Re (≡ circulation/kinematic viscosity) of 10000 is the second test case. As in the first test case, Figure 2 illustrates high similarity of results for all four discussed methods, especially in terms of the small-scale vortical substructures of connecting ribs of the reconnection process.

Flow Around an Inclined Flat Plate

The two examined datasets describe the impulsively started incompressible flow around an inclined flat plate (aspect ratio 2) at an angle of attack of 30 deg solved numerically for Reynolds numbers Re = 300 and Re = 1200. The results shown in Figure 3 indicate that the two explicit shear-eliminating methods (TDM and average-corotation scheme) are able—contrary to the widely used criteria Q and λ_2—to capture more adequately the vortical structures in close proximity of the flat plate (just behind the plate edges). The two popular methods, Q and λ_2, fail to correctly interpret the regions of high shear in the near wake: the shear zones are interpreted in a biased manner as vortical structures. These methods are less efficient in distinguishing vortex sheets formed at the plate edges from the sought swirling vortex rolls representing here a later stage of vortex sheet transformation.

Flow Around a Revolving Insect Wing

The vortex structure behind the wing of a fruit fly (*Drosophila*) revolving in a propellerlike motion is examined at the end of the first revolution. The flow is dominated by the spiraling tip vortex, enclosed by the starting leading-edge and trailing-edge vortices, and by a weaker vortex near the root of the wing. The angle of attack is fixed at 40 deg and the Reynolds number (based on the

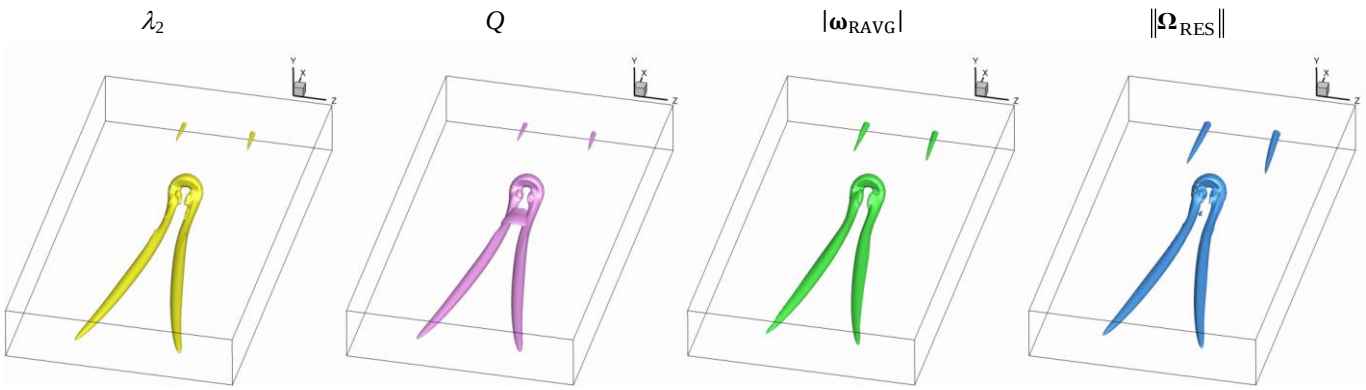

Figure 1. Hairpin vortex of boundary-layer transition.

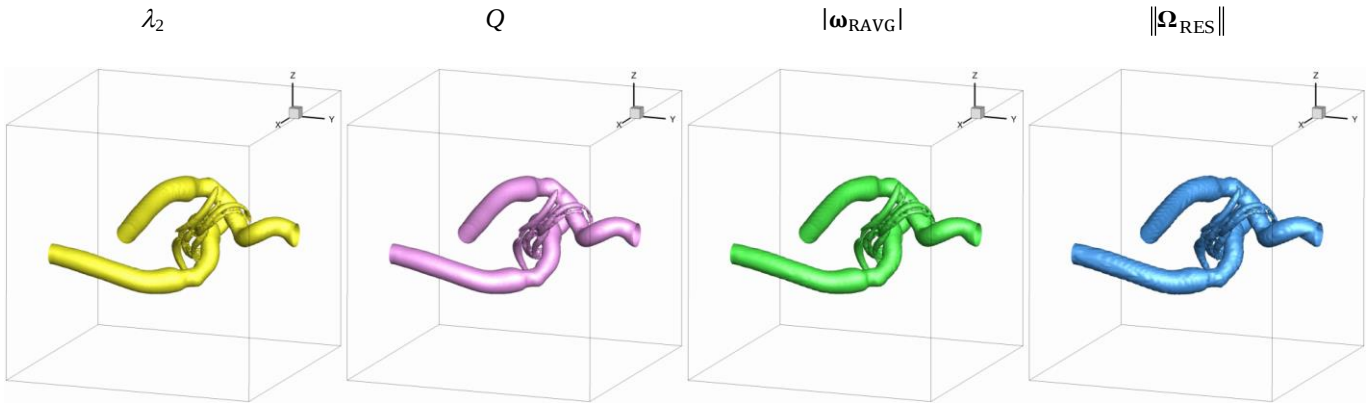

Figure 2. Interaction of two Burgers vortices.

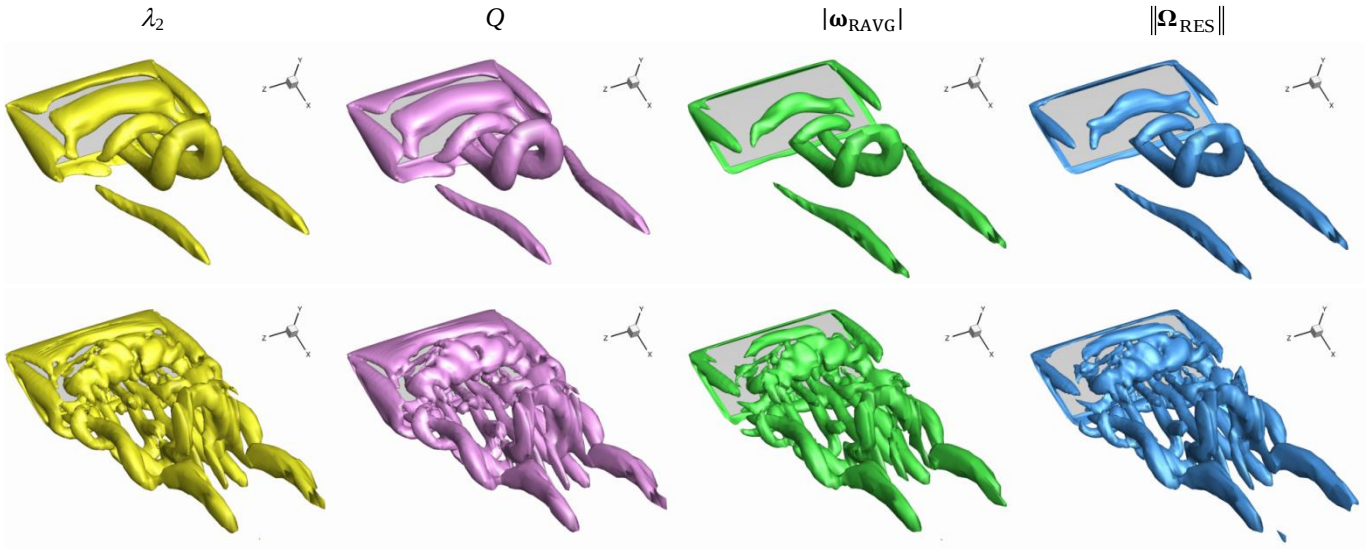

Figure 3. Vortical structures in the wake of an inclined impulsively started flat plate for Re = 300 (top) and Re = 1200 (bottom).

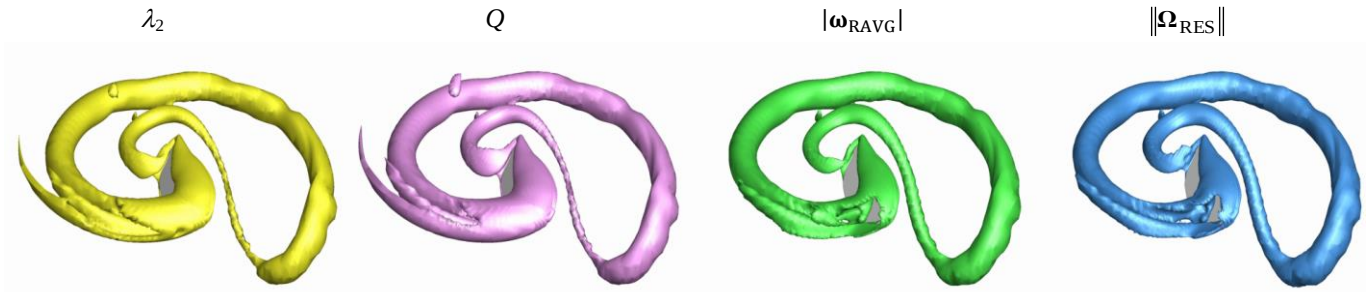

Figure 4. Vortical structures in the wake of a revolving wing of *Drosophila* for Re = 500.

velocity of the wing tip) is *Re* = 500. Similarly as in the case of the flow around an inclined flat plate, the widely used methods, Q and λ_2, tend in the very near wake of the wing to absorb some of the shear-based vorticity generated near the sharp wing edges as indicated in Figure 4. In addition, to analyze the results in Figure 4 from the viewpoint of shear, Figure 5 focuses on (the magnitude of) the vector of average-shear vorticity $\boldsymbol{\omega}_{\mathrm{SAVG}}$, for the definition see Appendix (the last part related to average-corotation method). It should be emphasized that this quantity absorbs the effect of both the *internal* shear and *external* shear. The *internal* shear which is inherent in a vortex means shearing motion of quasi-cylindrical layers inside a vortex, hence somewhat imitating vortical structure. The *external* shear is, at a given instant of time, virtually superimposed on the already generated vortex motion and represents a potential source of change in vortex dynamics and deformation. In the present case, both the *external* shear and vortices are generated behind the wing.

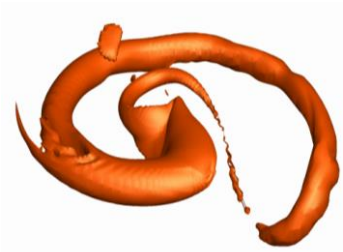

Figure 5. Revolving wing of *Drosophila*: average-shear vorticity $|\boldsymbol{\omega}_{\mathrm{SAVG}}|$.

For the sake of consistency, the threshold level of $|\boldsymbol{\omega}_{\mathrm{SAVG}}|$ depicted in Figure 5 is determined using precisely the same matching procedure as employed for the vortex-identification results (as briefly summarized at the beginning of this section).

A very close resemblance between $|\boldsymbol{\omega}_{\mathrm{SAVG}}|$ and the outcome of methods Q and λ_2, which can be inferred from Figures 4 and 5, indicates a shear bias of the two criteria.

Conclusions

Focusing on the bias due to shear, two explicit shear-eliminating vortex-identification methods, the TDM and the average-corotation scheme, have been compared with two popular schemes, Q and λ_2, which reduce the shear bias in an implicit manner. Four different flow situations (a hairpin vortex of boundary-layer transition, the reconnection process of two Burgers vortices, a flow around an inclined flat plate, and a flow around a revolving insect wing) have been analysed, and it has been found that the explicit shear-eliminating methods are more efficient in regions of strong shear. In the present study, such flow regions are formed in the near wake just behind the sharp edges of a plate or wing. Moreover, though the two explicit shear-eliminating schemes are clearly different in 3D (see Appendix for more information), the obtained results show surprisingly high similarity between these two methods regardless of the shear rate. The same conclusion holds for the outcome of the Q and λ_2 criteria within the present investigation.

Appendix

Q-criterion [1]: Vortices of an incompressible flow are identified as connected fluid regions with a positive second invariant of the velocity-gradient tensor $\nabla\mathbf{u}$, $\nabla\mathbf{u}=\mathbf{S}+\boldsymbol{\Omega}$, $\mathbf{S}$ is the strain-rate tensor, $\boldsymbol{\Omega}$ is the vorticity tensor (in tensor notation below, the subscript comma denotes differentiation),

$$Q \equiv \frac{1}{2}\left(u_{i,i}^2 - u_{i,j}u_{j,i}\right) = -\frac{1}{2}u_{i,j}u_{j,i} = \frac{1}{2}\left(\|\boldsymbol{\Omega}\|^2 - \|\mathbf{S}\|^2\right) > 0\,. \tag{A.1}$$

This is fulfilled in the regions where the vorticity magnitude prevails over the strain-rate magnitude. The additional pressure condition [1] requiring that the pressure tends to a minimum inside the region $Q > 0$ is arguable [2, 7, 11] and usually omitted.

λ_2-criterion [2]: This criterion is formulated on dynamic considerations, namely on the search for a pressure minimum across the vortex. The quantity $\mathbf{S}^2+\boldsymbol{\Omega}^2$ is employed as an approximation of the pressure Hessian after removing the unsteady irrotational straining and viscous effects from the strain-rate transport equation for incompressible fluids. A vortex region is defined as a connected fluid region with two negative eigenvalues of $\mathbf{S}^2+\boldsymbol{\Omega}^2$, that is, if the eigenvalues are ordered, $\lambda_1 \geq \lambda_2 \geq \lambda_3$, by the condition $\lambda_2 < 0$.

Triple-decomposition method (TDM) [8]: The TDM is expressed through the corresponding triple decomposition of a local motion near a point. As a result, $\nabla\mathbf{u}$ consists, unlike the double decomposition $\nabla\mathbf{u}=\mathbf{S}+\boldsymbol{\Omega}$, of three parts so that the strain-rate tensor $\mathbf{S}$ and vorticity tensor $\boldsymbol{\Omega}$ are cut down in magnitudes to share their portions through the third term $(\nabla\mathbf{u})_{\mathrm{SH}}$ associated with a local shearing motion. Consequently, in terms of the *residual* parts of $\mathbf{S}$ and $\boldsymbol{\Omega}$ it reads

$$\nabla\mathbf{u} = \mathbf{S}_{\mathrm{RES}} + \boldsymbol{\Omega}_{\mathrm{RES}} + (\nabla\mathbf{u})_{\mathrm{SH}}\,. \tag{A.2}$$

The first term on the right-hand side of (A.2) stands for an irrotational straining, the second one represents a rigid-body rotation. The third term of the triple decomposition denoted as $(\nabla\mathbf{u})_{\mathrm{SH}}$ and representing a shearing motion is described by a purely asymmetric tensor form—labelled *shear* tensor—fulfilling in a suitable reference frame (again, the subscript comma below denotes differentiation)

$$u_{i,j} = 0 \quad OR \quad u_{j,i} = 0 \quad (\text{for all } i, j)\,. \tag{A.3}$$

From the viewpoint of the double decomposition, $\nabla\mathbf{u}=\mathbf{S}+\boldsymbol{\Omega}$, the extracted term $(\nabla\mathbf{u})_{\mathrm{SH}}$ itself is responsible for a specific portion of vorticity and for a specific portion of strain rate.

The TDM is closely associated with the so-called "basic reference frame" (BRF). In this frame, the decomposition is performed in a clearly recognizable manner. However, the TDM results generated (i.e. separated) in the BRF are valid for all frames of reference rotated with respect to the BRF under an orthogonal transformation. The search for BRF presents an optimization problem for each point in the flow domain as briefly described in the following.

In the BRF: (i) the most effective shearing motion is described by the tensor form (A.3) under the defining condition that (ii) the effect of extraction of a *shear* tensor is maximized within the following decomposition scheme applicable to an arbitrary reference frame

$$\nabla\mathbf{u} \equiv \begin{pmatrix} u_x & u_y & u_z \\ v_x & v_y & v_z \\ w_x & w_y & w_z \end{pmatrix} = \begin{pmatrix} residual \\ tensor \end{pmatrix} + \begin{pmatrix} shear \\ tensor \end{pmatrix} \tag{A.4}$$

where the *residual* tensor is defined as

$$\begin{pmatrix} u_x & (\mathrm{sgn}\,u_y)\,\mathrm{MIN}\left(|u_y|,|v_x|\right) & \bullet \\ (\mathrm{sgn}\,v_x)\,\mathrm{MIN}\left(|u_y|,|v_x|\right) & v_y & \bullet \\ \bullet & \bullet & w_z \end{pmatrix}. \tag{A.5}$$

The following notation is used in (A.4) and (A.5): *u*, *v*, *w* are velocity components, subscripts *x*, *y*, *z* stand for partial derivatives. The remaining non-specified pairs of off-diagonal elements of the *residual* tensor in (A.5) are constructed analogously as the specified one, each pair—if considered separately—being either symmetric or antisymmetric. The effect of extraction of the *shear* tensor is maximized by changing the reference frame under an orthogonal transformation so that the absolute tensor value of the *residual* tensor is minimized, or the closely related scalar quantity $|S_{12}\Omega_{12}|+|S_{23}\Omega_{23}|+|S_{31}\Omega_{31}|$ is maximized, as shown in [8]. This extremal condition guarantees that an effective shearing motion is recognized in the BRF as a third elementary part of the triple decomposition and can be extracted from $\nabla\mathbf{u}$ following (A.4) and (A.5). For details and the qualitative description of the flow kinematics near a point adopted in the TDM, see [8].

The *residual* vorticity tensor $\mathbf{\Omega}_{\mathrm{RES}}$ representing a rigid-body rotation in 3D is assumed to provide an "unbiased shear-free measure" of the actual swirling motion of a vortex. Finally, according to TDM, non-zero magnitude (i.e. Frobenius norm) of $\mathbf{\Omega}_{\mathrm{RES}}$, $\|\mathbf{\Omega}_{\mathrm{RES}}\|>0$, identifies the examined point as part of a vortex. Earlier 3D applications of this method can be found in [12, 13]. An analysis of cross sections of vortices in turbulent flows using TDM is presented in [14], and another application of the planar residual vorticity has been recently described in [15].

The average-corotation method [9]: The scheme is based on the two following steps: Firstly, the local corotation of material line segments at a point is defined on a 2D plane. This planar concept is directly related to the residual vorticity in 2D according to the above-mentioned TDM as the residual vorticity is a measure of local planar corotation of material line segments. Secondly, a proper averaging process is applied to all planar cross sections going through the given point. The averaging procedure is performed as surface integration over a unit sphere, which is approximated using numerical quadrature from [16].

The integral over a unit sphere can be expressed using the spherical coordinates *r*, φ, ϑ as a double integral

$$\boldsymbol{\omega}_{\mathrm{RAVG}}=\frac{\alpha}{4\pi}\int_0^{2\pi}\int_0^{\pi}\boldsymbol{\omega}_{\mathrm{RES}}\left(\mathbf{x}_0,\mathbf{n}(\varphi,\vartheta)\right)\sin\vartheta\,\mathrm{d}\vartheta\,\mathrm{d}\varphi \qquad (A.6)$$

where $\boldsymbol{\omega}_{\mathrm{RAVG}}$ denotes the average-corotation vector, $\boldsymbol{\omega}_{\mathrm{RES}}$ is the planar residual vorticity determined according to TDM and oriented as the plane normal $\mathbf{n}$, and $\mathbf{x}_0$ denotes the examined point. A natural choice $\alpha = 3$ is derived from the requirement that average-corotation vector equals to vorticity vector, $\boldsymbol{\omega}_{\mathrm{RAVG}}=\boldsymbol{\omega}$, for a pure rotational motion $\nabla\mathbf{u}=\mathbf{\Omega}$.

To evaluate the contribution of shearing motion to vorticity separately, the vector of average-shear vorticity $\boldsymbol{\omega}_{\mathrm{SAVG}}$ has been introduced in [9] and given simply by the resulting formula

$$\boldsymbol{\omega}_{\mathrm{SAVG}}=\boldsymbol{\omega}-\boldsymbol{\omega}_{\mathrm{RAVG}}\,. \qquad (A.7)$$

Note that the expression (A.7) is obtainable by the analogous averaging procedure as $\boldsymbol{\omega}_{\mathrm{RAVG}}$.

Finally, the magnitude of the vector $\boldsymbol{\omega}_{\mathrm{RAVG}}$ can be employed in 3-D vortex identification as already shown in [9] where $|\boldsymbol{\omega}_{\mathrm{RAVG}}|$ has been employed for region-type identification of a vortex in the same manner as presented here.

Acknowledgments

The authors are very grateful to Ulrich Rist and Kudret Baysal, Institute of Aerodynamics and Gasdynamics, University of Stuttgart, for some of the direct numerical simulation datasets used in the present paper. The authors are also grateful to Fehmi Cirak, Department of Engineering, University of Cambridge, for providing his computational codes for obtaining datasets used in this paper as well as for valuable discussions on the subject. This work was supported by the Czech Science Foundation through grant 14-02067S, and by the Academy of Sciences of the Czech Republic through RVO:67985874 and RVO:67985840.

References

[1] Hunt, J.C.R., Wray, A.A. & Moin, P., Eddies, Streams, and Convergence Zones in Turbulent Flows, *Center for Turbulence Research Report CTR*-S88, 1988, 193–208.

[2] Jeong, J. & Hussain, F., On the Identification of a Vortex, *J. Fluid Mech.*, **285**, 1995, 69–94.

[3] Dallmann, U., Topological Structures of Three-Dimensional Flow Separation, *Deutsche Forschungs- und Versuchsanstalt für Luft- und Raumfahrt DFVLR-IB Report* No. 221–82 A07, 1983.

[4] Vollmers, H., Kreplin, H.-P. & Meier, H.U., Separation and Vortical-Type Flow Around a Prolate Spheroid — Evaluation of Relevant Parameters, *Proceedings of the AGARD Symposium on Aerodynamics of Vortical Type Flows in Three Dimensions*, Rotterdam, Netherlands, AGARD-CP-342, Apr. 1983, pp. 14-1–14-14.

[5] Chong, M.S., Perry, A.E. & Cantwell, B.J., A General Classification of Three-Dimensional Flow Fields, *Phys. Fluids A*, **2**, 1990, 765–777.

[6] Zhou, J., Adrian, R.J., Balachandar, S. & Kendall, T.M., Mechanisms for Generating Coherent Packets of Hairpin Vortices in Channel Flow, *J. Fluid Mech.*, **387**, 1999, 353–396.

[7] Chakraborty, P., Balachandar, S. & Adrian, R.J., On the Relationships Between Local Vortex Identification Schemes, *J. Fluid Mech.*, **535**, 2005, 189–214.

[8] Kolář, V., Vortex Identification: New Requirements and Limitations, *Int. J. Heat Fluid Flow*, **28**, 2007, 638–652.

[9] Kolář, V., Šístek, J., Cirak, F. & Moses, P., Average Corotation of Line Segments Near a Point and Vortex Identification, *AIAA J.*, **51**, 2013, 2678–2694.

[10] Bake, S., Meyer, D.G.W. & Rist, U., Turbulence Mechanism in Klebanoff Transition: a Quantitative Comparison of Experiment and Direct Numerical Simulation, *J. Fluid Mech.*, **459**, 2002, 217–243.

[11] Cucitore, R., Quadrio, M. & Baron, A., On the Effectiveness and Limitations of Local Criteria for the Identification of a Vortex, *Eur. J. Mech. – B/Fluids*, **18**, 1999, 261–282.

[12] Kolář, V., Moses, P. & Šístek, J., Triple Decomposition Method for Vortex Identification in Two-Dimensional and Three-Dimensional Flows, in *Computational Fluid Dynamics 2010*, editor A. Kuzmin */Proc. of the 6th International Conference on Computational Fluid Dynamics*, St. Petersburg (Russia), 2010/, 225–231, Springer 2011.

[13] Šístek, J., Kolář, V., Cirak, F. & Moses, P., Fluid-Structure Interaction and Vortex Identification, in *Proceedings of the 18th Australasian Fluid Mechanics Conference*, editors P.A. Brandner and B.W. Pearce, Launceston (Australia), Paper 125, Australasian Fluid Mechanics Society 2012.

[14] Maciel, Y., Robitaille, M. & Rahgozar, S., A Method for Characterizing Cross-Sections of Vortices in Turbulent Flows, *Int. J. Heat Fluid Flow*, **37**, 2012, 177–188.

[15] Peltier, Y., Erpicum, S., Archambeau, P., Pirotton, M. & Dewals, B., Meandering Jets in Shallow Rectangular Reservoirs: POD Analysis and Identification of Coherent Structures, *Exp. Fluids*, **55**, 2014, 1740-1–1740-16.

[16] Hannay, J.H. & Nye, J.F., Fibonacci Numerical Integration on a Sphere, *J. Phys. A: Math. Gen.*, **37**, 2004, 11591–11601.